Assessment of the Robustness of Flexible Antennas to Complex Deformations

Ekrem Altinozen, *Graduate Student Member, IEEE,* Ana Vukovic, *Member, IEEE,* Phillip Sewell

***Abstract*—Wearable antennas can suffer from a variety of mechanical deformations that are induced by the body dynamic. The paper analyses how these complex deformations impact the performance of a flexible antenna operating in the 5-6 GHz band. The Green Coordinates spatial manipulation technique is used to generate a range of complex two-dimensional deformations, namely spherical, saddle, and twisting deformation. Generating full geometries is a key enabler in this study. The results offer valuable insight to the stability of antenna performance under in-situ deformations.**

***Index Terms*— computer graphics, flexible antenna, microstrip antenna, numerical modelling.**

I. Introduction

THE next-generation wireless communication systems have increased the demand for flexible and wearable antennas for a variety of applications ranging from sport to biomedical. Considerable research has been focused on developing flexible substrates [1, 2], and intrinsically stretchable conductors [3-6]. It is now well established that the polydimethylsiloxane (PDMS) polymer is one of the most promising substrate materials for wearable electronics due to its high conformability compared to other polymer types, adjustable relative permittivity, acceptable dielectric losses and low-cost fabrication methods [2, 7, 8]. In addition to PDMS substrates, textile substrates, such as e-textile, woven and knitted textile structures are favorable alternatives [9-12] but exhibit lower stability in combination with conductive prints and limited design performance predictability due to complex geometrical details of conductive threads [9-14].

Integration of antennas into clothing means that the antennas will be affected by the dynamics of the human body that can cause a variety of deformations [15-19] which in turn can degrade the overall system's performance and present a challenging design task for wearable antenna design.

One major issue in the design of wearable antennas is the fact that they are initially designed as flat components. The impact of deformations are predominantly assessed by assuming that antennas are bent in situ along a cylindrical plane, primarily using experimental measurements [2, 3, 19-24] and less frequently using commercial software such as Ansys and CST [21, 22, 24-26].

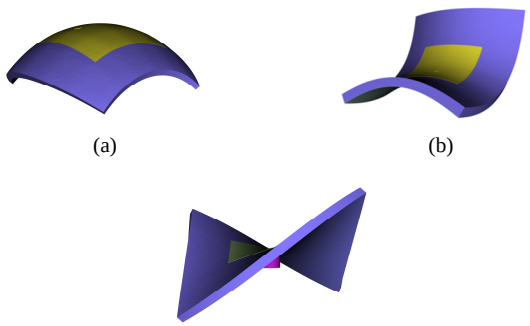

Fig.1. Two-dimensional deformations of antenna – example of a) spherical bending, b) saddle and c) twisting deformations.

Although there are numerous, unfortunately often conflicting, results on the impact of cylindrical bending on antenna performance, it is now widely accepted that bending antennas along antenna length is more critical for performance as it increases the resonant frequency of antennas [20, 21, 24]. The bending does not significantly affect the bandwidth of antenna or the far field radiation pattern [20, 21, 24]. More recently, the impact of twisting on flexible interconnects [27] and wideband dipole antennas [17] was reported showing a small impact on their performance.

However, the impact of other types of deformations, in particular more complex two-dimensional (2D) deformations, such as spherical, saddle and twisting deformations as shown in Fig.1, have not been considered. The focus on simpler cylindrical deformations is due to the fact that it is relatively straightforward to generate these geometries in standard computational electromagnetic (EM) software, such as Ansys and CST, that are based on Constructive Solid Geometry (CSG) primitives and Boolean geometry. It is commented here that the subsequent choice of modelling method, Finite Elements, Finite Integration Technique, Method of Moments, or their

This paragraph of the first footnote will contain the date on which you submitted your paper for review. It will also contain support information, including sponsor and financial support acknowledgment. For example, “This work was supported in part by the U.S. Department of Commerce under Grant BS123456”.

The next few paragraphs should contain the authors’ current affiliations, including current address and e-mail. For example, F. A. Author is with the National Institute of Standards and Technology, Boulder, CO 80305 USA (e-mail: author@ boulder.nist.gov).

S. B. Author, Jr., was with Rice University, Houston, TX 77005 USA. He is now with the Department of Physics, Colorado State University, Fort Collins, CO 80523 USA (e-mail: author@lamar.colostate.edu).

T. C. Author is with the Electrical Engineering Department, University of Colorado, Boulder, CO 80309 USA, on leave from the National Research Institute for Metals, Tsukuba, Japan (e-mail: author@nrim.go.jp).

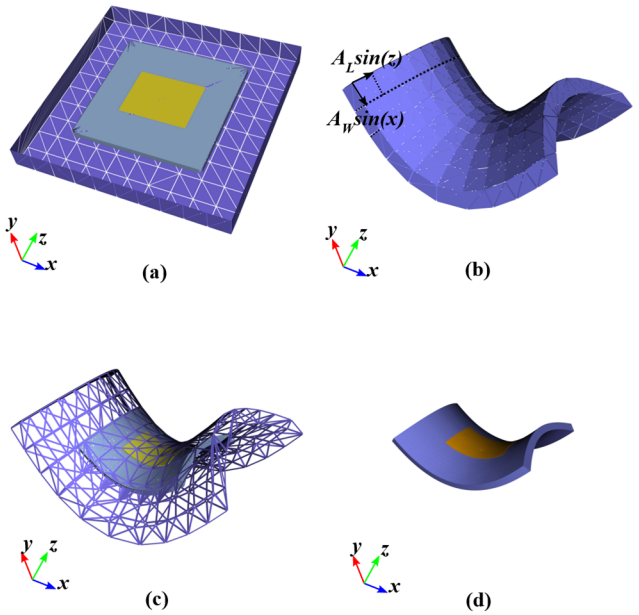

Fig.2. GC methodology: a) flat antenna within a flat cage (only faces of the flat cage are shown); b) warped cage that describes the nature of the deformation; c) deformed antenna inside the warped cage (only edges of the warped cage shown) and d) final geometry of a deformed antenna.

implementation within particular software packages is not the issue, rather it is the geometrical data upon which they operate that has the failing. The main difficulty when generating arbitrary deformations is in obtaining well behaved interfaces between the constitutive parts of the antenna, free of misalignments and microscopic gaps, as discussed in [28-30], which can undermine subsequent EM numerical simulations. Our recent work [28] proposed the use of a computer graphics spatial manipulation technique based on Green Coordinates (GC) for generating arbitrary deformations of antennas [31,32]. The GC technique belongs to a class of cage-based methods that enclose the object of interest by a so-called bounding cage that has a similar, but less complicated shape than the object of interest. The GC method stands out from other similar spatial manipulation techniques (Mean Value Coordinates [33, 34], and Harmonic Coordinates [33]) as it is the most shape-preserving, i.e., introduces a *minimal* amount of unphysical *distortions* and is computationally efficient as is implemented using a closed-form analytical expression [31, 32]. Our recent work demonstrated that GC method provides a robust approach *to generating highly variable geometries* of deformed antennas without introducing the disruptive CAD artefacts that can either block or seriously undermine EM characterization.

The systematic distortions that are introduced by the GC method can be effectively compensated for by using an iterative pre-scaling approach, as shown in [28-30], that guarantees physical reality of the final geometries. This approach was calibrated against the simple case of cylindrical bending for which no distortion is expected to occur and proved that the performance of the GC generated cylindrically bent antenna agrees well with the CSG generated antennas opening the way for robust generation of more general antenna deformations [28]. A few representative complex, double curved antenna geometries have been demonstrated in [28] but a more general analysis of antenna performance under varying degrees of these complex deformations is needed in order to: a) assess the general sensitivity of an antenna to a variety of deformations, b) identify which class of deformations have the most disruptive impact on the antenna performance and c) investigate whether simpler cylindrical deformations can indeed be used to predict the impact of more complex deformations.

This paper extends the approach of [28] to consider a more systematic parameter sweep of the problem space for several cases of doubly curved deformations, namely, spherical and saddle bending and twisting deformation. Although these still do not span all “irregular” deformations, they are in nature more complex than the simpler case of cylindrical bending. Specifically, the paper explores how these deformations affect the performance of flexible antenna fabricated on PDMS substrates operating in the 5.5-6 GHz wireless band.

The paper is structured as follows: Section II briefly overviews the GC method in the context of arbitrary antenna generation and defines the parameters of the warped cages for spherical, saddle and twisting deformations. Section III assesses the impact of spherical, saddle, and twisting deformation on antenna performance, namely S_{11}, bandwidth and far field profile. This section further investigates whether the impact of 2D antenna deformations can be predicted by simpler cylindrical deformations. Section IV gives the overall conclusions of the paper.

II. Complex Antenna Deformations

In this section the main principle of the GC method is overviewed and applied to a variety of complex 2D antenna deformations.

The GC technique belongs to a type of cage-based methods that enclose the object of interest by a so-called bounding cage that has a similar, but less complicated shape than the object of interest, and, as shown in Fig. 2a), for the case of patch antenna the bounding cage is a simple polygonal tube [28-30]. All spatial points within the interior of the cage can be expressed in terms of the cage’s geometry e.g. vertices and face normals of the cage’s surface triangulations [28-30]. The vertices of the simple cage are then manipulated to generate a wanted deformation as shown in Fig. 2b) for the case of saddle deformation. The deformation of the cage is then mapped onto the geometry of the enclosed object, as shown in Fig. 2c). Removing the warped cage leaves the deformed object, as shown in Fig. 2d). It is a highly valuable feature of the GC method that it maps relatively crudely defined deformations of the warped cage onto the smooth deformations of the final geometry, beyond the scope of explicit manual intervention.

For the patch antenna with a coaxial feed two approaches can be adopted when constructing the flat cage namely, a) construct the cage that follows the shape of antenna and antenna cross section that includes the extrusion around the coaxial cable. That part of the cage that surrounds the coaxial feed does not experience any deformation, but the rest of the cage is deformed as required, or, b) define the flat cages as shown in Fig.2a), i.e.

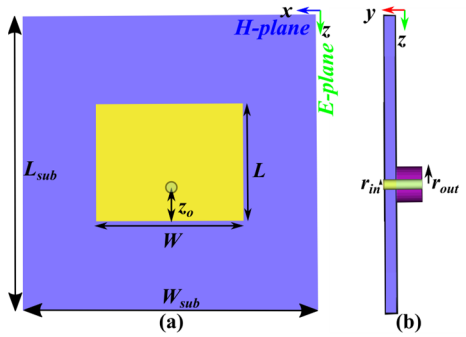

Fig. 3. The flat patch antenna geometry, a) the top view of antenna where the x-axis is the H-plane of the antenna and z-axis is the E-plane of the antenna; b) the side view where the y-axis is the propagation direction of the excitation pulse.

a simple polyhedron, deform the cage as required, and then add the coaxial cable to the deformed antenna using Boolean "through" operation. In this paper the latter approach is used due to the controlled nature of deformations. However, in case of more general or irregular deformations the former approach may be better suited.

The GC method opens a way of generating more complex antenna deformations and these will now be investigated on a typical example of wearable patch antenna fabricated on a flexible PDMS substrate and operating in the wireless 5.5-6GHz band. The schematic of the flat patch antenna is shown in Fig. 3. The substrate's length, L_{sub}, width, W_{sub}, and thickness, h, are 36 mm, 36 mm and 1.5 mm respectively. The metallic patch has width, W=18 mm, and length, L= 14.3 mm. The feed position is offset by z_o=2.8 mm in the z- direction from the middle of the patch and is designed to give an optimal S_{11} parameter of antenna and 3.5% of fractional bandwidth. The coaxial cable feed has inner, r_{in}, and outer radius, r_{out} of 0.625 mm and 2.15 mm respectively. The cable dielectric constant is 2.2. The dielectric constant of the PDMS substrate is 2.7 and its dielectric losses are neglected. The radiating patch and the ground plane are assumed to be perfect conductors of 35 μm thickness.

Fig. 4 illustrates the cages that are considered in this paper. In all cases the flat cage width, length and height are 56 mm, 56 mm and 7.5 mm respectively and the antenna is positioned in the center of the flat cage. The concave and convex spherical deformations are characterized by a spherical radius, r. To generate these spherical deformations a cross-section of a polygonal tube is defined and then extruded along the width or the length of the cage (Fig. 4a)). By changing the origin of the sphere, i.e. above or below the top antenna surface, the concave and convex deformations can be obtained and the radius of the sphere defines the strength of imposed deformation.

Similarly, to generate saddle deformations a cross-section of a polygonal tube is defined across the width (length) of the cage as a sinusoidal parabola and the tube is extruded along the length (width) along a defined parabola. Fig.4c) shows an example of a saddle cage where the saddle deformation of the cage is controlled by the half period of the sine function $A_W sin(x)$ along the width of antenna and $A_L sin(z)$ along the length of antenna. The strength of the deformation is controlled by the parameter A_W and A_L with the peak value centered at

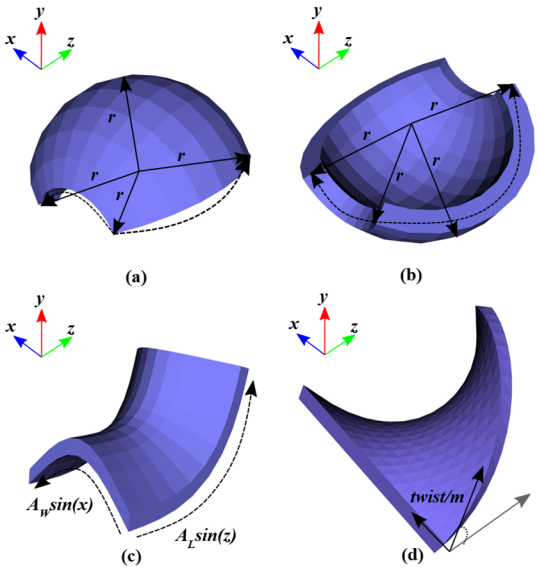

Fig. 4. Warped cages describe the nature and level of deformation for generating (a) concave (b) convex (c) saddle and (d) twisting deformation.

the midpoint along the width and length of the cage respectively. Saddle deformations are obtained when amplitudes A_W and A_L have opposite signs. Finally, the twisting deformation is generated by defining a cross section of the cage which is then extruded and twisted along the length or width of antenna, Fig.4d), with a twisting deformation controlled by a mean twist per meter parameter.

To re-assure the reader of the accuracy of the GC method in the context of 2D deformations, Fig. 5 shows the relative distortion in the length and width of the radiating patch. The iterative pre-scaling approach described in [28-30] is applied to each deformation namely the spherical convex (r = 30 mm), saddle (A=A_W=A_L=20 mm) and twisting (0.0125 twist/m) deformations. It can be seen that relative distortion is initially high but rapidly reduces after only a few iterations. Fig.5 also shows that distortion errors for the spherical and twisting deformations reduce more rapidly than for the case of saddle deformation.

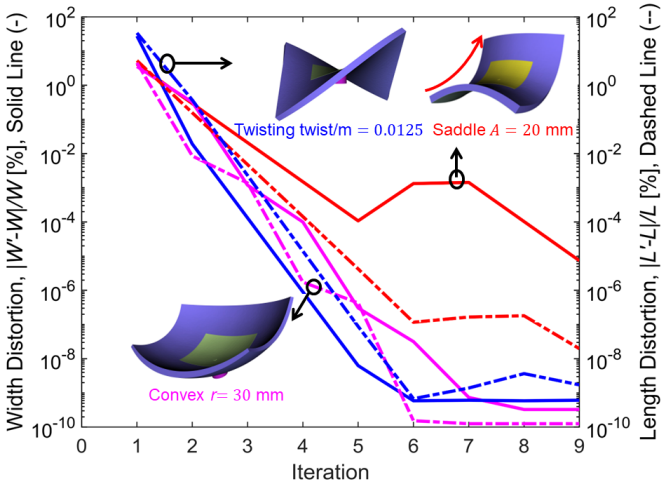

Fig.5 GC induced relative distortion error in the width (solid line) and length (dashed line) of the radiating patch as a function of number of pre-scaling iterations for generating convex, saddle and twisting antenna deformations.

III. DEFORMED ANTENNA PERFORMANCE

In this section the impact of complex deformations on antenna performance, namely on antenna resonant frequency, reflection coefficient and bandwidth, is investigated. The change in material properties of the antenna substrate and the metallic patch due to deformations is not included in the model.

The generated geometries of deformed antennas are imported into in-house time-domain electromagnetic (EM) solver based on Transmission Line Modelling (TLM) method [37] and tetrahedral Delaunay meshing [38]. The tetrahedral TLM method [38] is a well-established extension of the Cartesian TLM method [37], and has been demonstrated to be second-order accurate with respect to wavelength, provides both smooth boundary and

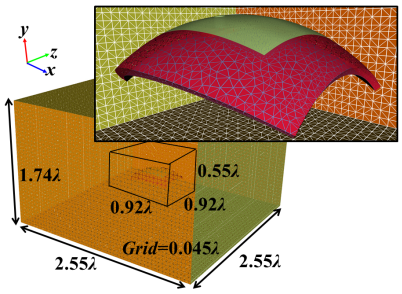

Fig. 6. Computational box with antenna, depicting the fictitious box in the near field of antenna that is meshed more finely. The inset of the figure depicts the hybrid mesh of the concave antenna.

graded mesh capabilities and has been industrially characterized and deployed for a range of applications, including EMC and aerospace [39-42]. Space precludes a more detailed description of the method and readers are specifically referred to [38, 39] for further details.

In all cases the whole problem is meshed with a hybrid mesh that is a combination of a 2.5 mm cubic mesh and a tetrahedral mesh. The antenna near field is meshed more finely with 0.625 mm hybrid mesh as described in [40]. The antenna near field region is captured in a fictitious box of size 0.92 λ × 0.92 λ × 0.55 λ, where λ is the operating wavelength of 5.5 GHz. A free space impedance boundary condition is imposed on the boundaries of the computational box. An example of the meshed computational problem is given in Fig. 6 where the inset in Fig.6 gives a closer view of the sampled antenna surface within the computational box. In all cases the antenna is excited with the fundamental TEM mode of the coaxial feed modulated by a time-domain pulse with 3 dB frequencies of 4.6 and 7 GHz. The fundamental TEM mode is obtained as an eigen solution of the discretized 2D cross section of the coaxial cable [43]. All simulations are run on 8 processor cores of a commodity cluster for 2 million time steps. The threshold for forming cell clusters is 5 μm and the timestep is 0.018 ps [39]. The performance of the flat patch antenna is taken as a reference with a resonant frequency of 5.68 GHz, reflection coefficient (S_{11}) at the resonant frequency of -30.6 dB and fractional bandwidth of 3.5%.

A. *Spherical Convex and Concave Deformations*

In this section the impact of spherical convex and concave deformations on antenna performance is considered. The flat antenna is generated using Boolean geometry. To achieve desired spherical deformation the deformed cage is generated by placing the origin of the sphere below (concave) or above (convex) the antenna ground plane and the cage cross section is extruded along the length of the antenna. The deformation of the cage is controlled by the radius parameter as shown in Fig.4a,b) with the radius varying from 50 mm to 20 mm for the concave case and from 50 mm to 30mm for the convex case.

Fig. 7 shows the impact of the spherical concave and convex deformation on the change of the resonant frequency compared to the resonant frequency of the flat antenna, f_0. The dB values in the figure denote the value of the S_{11} parameter at the resonant frequency for the given spherical radius and the shaded region defines the 3.5% fractional bandwidth of the flat antenna. The inset of the figure shows the deformed antenna geometries for selected spherical radii, namely r =50 mm, 30 mm and 20 mm, where the reduction of the radius corresponds to increased deformation. It can be seen that in the case of both convex and concave bending the resonant frequency increases with increased deformation. The concave deformation can cause up to 5% shift of the antenna resonant frequency whilst the antenna resonant frequency is less sensitive to the convex spherical deformation. In all cases the S_{11} value at the resonant frequency stays below -24 dB as indicated in Fig. 6. Furthermore, it can be seen that for deformation radius smaller than 30 mm the concave antenna performance moves outside the operating bandwidth of the flat antenna which is a key practical observation. This can be intuitively explained by the fact that the spherical bending acts so as to reduce the effective length of antenna. This effect is stronger in the case of concave bending whilst in the case of convex bending, the fringing fields at radiating edges act to counteract this effective length reduction resulting in smaller change in resonant frequency.

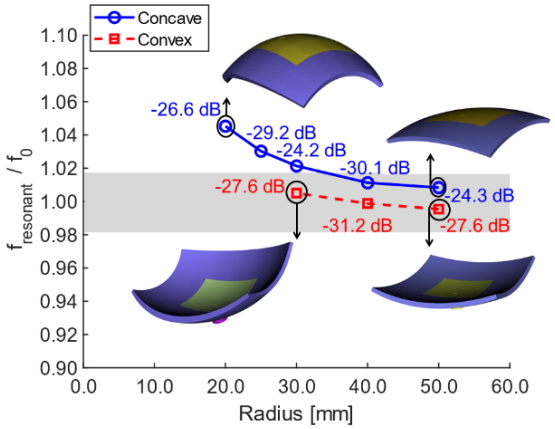

Fig. 7. Impact of the spherical concave and convex deformation on the resonant frequency of the deformed antenna compared to that of the flat antenna (f_0) for different spherical radii. Values (dB) indicate the value of S_{11} parameter at the resonant frequency and the shaded region indicates the 3.5% fractional bandwidth of the flat antenna.

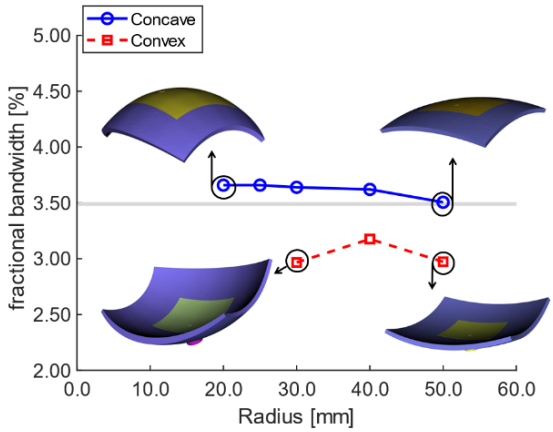

Fig.8. Impact of the spherical concave and convex deformations on the fractional bandwidth of the deformed antenna.

Fig.8 shows the impact of the concave and convex spherical deformations on the fractional bandwidth of antenna. The blue horizontal line denotes the 3.5% fractional bandwidth of the flat antenna. It can be seen that concave deformation marginally increases the bandwidth of antenna (up to 0.2%) whilst the convex deformation has the opposite effect on antenna bandwidth and results in bandwidth reduction (up to 0.5%). This may be explained by the fact that the fringing fields in the case of concave bending essentially decrease the effective dielectric constant which in turns increases the bandwidth of the antenna whilst the opposite is happening in the case of convex bending.

The impact of the spherical deformation on the far field radiation pattern is shown in Fig. 9. Fig. 9(a) compares the E-plane radiation pattern of the flat patch antenna (solid line) with the convex and concave spherically deformed antenna for the radius $r = 30$ mm (doted lines). Fig. 9(b) shows the same information but for the H-plane radiation pattern. It can be seen that convex and concave deformations do not significantly affect the main beam in the E-plane, with the main change being in the increased sidelobes. However, for the H-plane radiation pattern, the concave deformation increases both the main beam and the sidelobes whilst the convex spherical deformation slightly reduces the width of the main beam and increases the width and strength of the sidelobe. Again, the concave deformation is shown to affect the radiation pattern more which can be explained by that fact that fringing fields contribute to the increased sidelobe radiation.

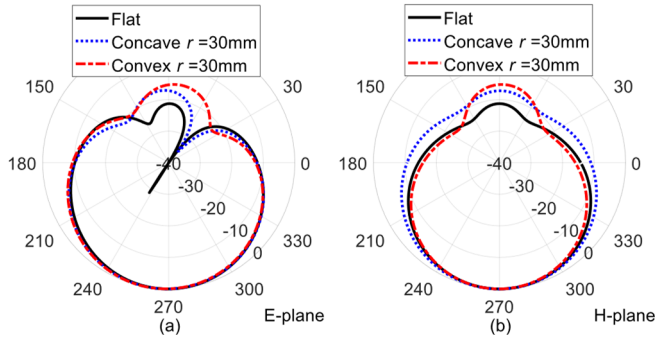

Fig. 9. Comparison of the far field radiation pattern at 5.6 GHz in a) E-plane and b) H-plane of a flat patch antenna (solid line) with antenna deformed using spherical concave deformation with r = 30 mm, (dotted line) and antenna deformed using spherical convex deformation with r = 30 mm (dashed line).

B. *Saddle Deformations*

In this section the impact of the 2D saddle deformations on antenna performance is considered. The cage for the saddle deformation is constructed as in Fig. 4c) and the strength of the deformation is controlled by the parameter $|A_W|=|A_L|=A$ that is varied from 0 mm (flat case) to 20 mm. Two cases are considered, namely when convex bending is along the width of antenna (concave bending is along the length of antenna) and when convex bending is along the length of antenna (concave bending is along the width of antenna).

The impact of saddle deformations on the change of resonant frequency compared to the resonant frequency of the flat case is shown in Fig. 10. As before, the dB values in the figure indicate the valued of the S_{11} parameter for given deformation and the shaded region defines the 3.5% fractional bandwidth of the flat antenna. It can be seen that convex bending along the width increases the antenna resonant frequency by up to 2%, whilst the convex bending along the length of antenna causes reduction in the antenna resonant frequency by up to 4% and moves it outside the operating bandwidth of the flat antenna. This can be explained by the fact that convex bending along the antenna width (and concave along the antenna length) acts to reduce the effective length of the antenna resulting in increased resonant frequency. On the other hand, convex bending along antenna length (and concave along the antenna width) means that fringing fields can act to increase the effective length of antenna and consequently decrease the antenna's resonant frequency. Moreover, the value of the S_{11} parameter at the antenna resonant frequency decreases to -9.9 dB resulting in the antenna not meeting the bandwidth requirements. This implies that convex nature of the deformation along the length of antenna is more critical for antenna resonant frequency.

Fig. 11 shows the impact of saddle deformations on the fractional bandwidth of antenna. It can be seen that convex deformation along the width of antenna generally reduces the operating bandwidth of antenna, whilst the convex deformation

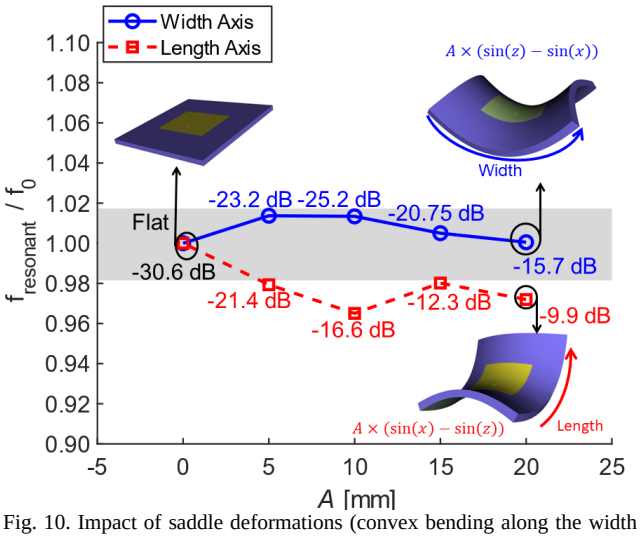

Fig. 10. Impact of saddle deformations (convex bending along the width and length of antenna) on the resonant frequency of deformed antenna compared to the resonant frequency of the flat antenna, f_0, Values (dB) indicate the value of S_{11} parameter at the resonant frequency and the shaded region indicates the 3.5% fractional bandwidth of the flat antenna.

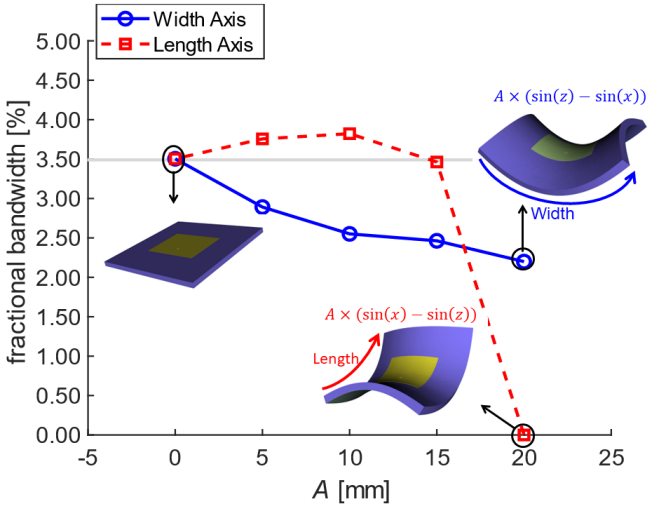

Fig. 11. Impact of the saddle deformations (convex bending along the width and length of antenna) on the fractional bandwidth of antenna.

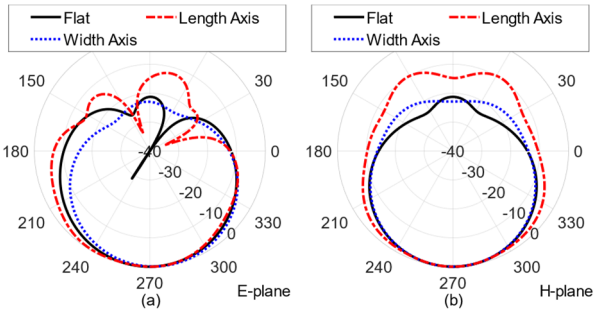

Fig. 12. Comparison of the far field radiation pattern at 5.6 GHz in a) E-plane and b) H-plane of a flat patch antenna (solid line) with antenna deformed using saddle deformation with convex bending along the length (dashed line) and along the width (dotted line) with A = 20 mm.

along the length slightly increases the bandwidth. However, Fig.10 also shows the increase in the S_{11} value at the resonant frequency that can be attributed to the changes in the bandwidth of antenna. Particularly in the case of convex deformation along the length of the antenna, the value of S_{11} at the resonant frequency increases with deformation, as shown in Fig.10, and results in a complete loss of bandwidth for stronger deformations.

The impact of saddle deformations on the far field radiation pattern is shown in Fig. 12. Fig.12(a) compares the E-plane radiation pattern of the flat patch antenna (solid line) with the deformed antenna for A=20 mm (doted lines). Fig.12(b) shows the same information but for the H-plane radiation pattern. It can be seen that saddle deformation with convex deformation along the length of antenna is more critical as it contributes to an increase of the main beam width as well as the sidelobe level. Saddle deformation with convex deformation along the width of antenna is seen to reduce the main radiation beam in the E-plane compared to the flat antenna. This can be explained by the complex interplay between fringing fields at antenna radiating edges that act to increase the radiated power in the sidelobes and also contribute to asymmetric radiation profile.

C. Twisting Deformations

In this section the impact of the twisting deformation on antenna performance is investigated. Twisting deformations are

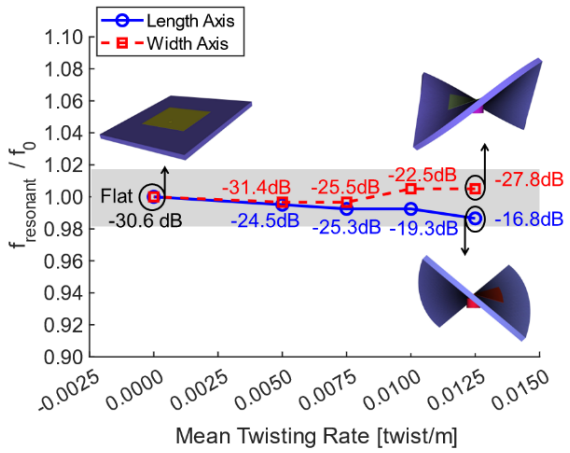

Fig. 13. Impact of twisting deformation applied along the width and length of antenna on the resonant frequency of deformed antenna compared to that of the flat antenna, f_0. Values (dB) indicate the value of S11 parameter at the resonant frequency and the shaded region indicates the 3.5% fractional bandwidth of the flat antenna.

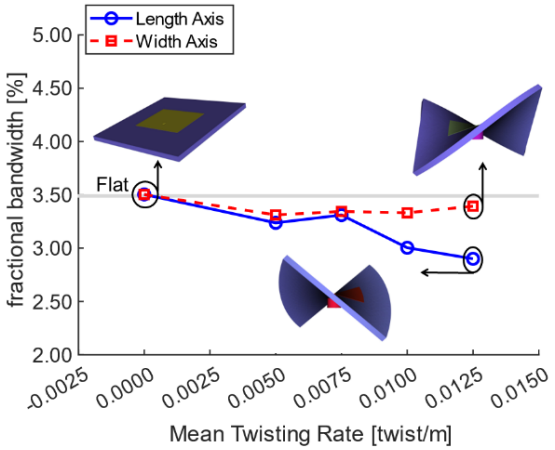

Fig. 14. Impact of the twisting deformation applied along the length and width of antenna on the fractional bandwidth of antenna.

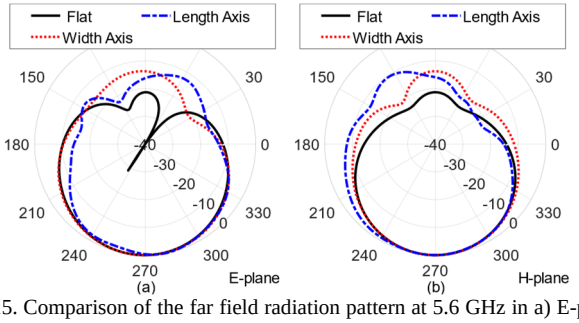

Fig. 15. Comparison of the far field radiation pattern at 5.6 GHz in a) E-plane and b) H-plane of a flat patch antenna (solid line) with antenna deformed using twisting deformation with 0.0125 twist/m along the length (dashed line) and along the width (dotted line) of antenna

imposed on the warped cage by specifying mean rotating per meter along the width and length of the antenna ranging from 0.0050 twist/m to 0.0125 twist/m.

Fig. 13 shows the ratio of the resonant frequency of the deformed antenna to that of the flat antenna for twisting deformation along length and width of antenna. It can be seen that increasing the twisting along the width of antenna increases the resonant frequency by about 1 % whilst twisting along the length of antenna decreases the resonant frequency by about 2%. This implies that twisting deformation along the length of

the antenna tends to increase the effective length of antenna resulting in a higher resonant frequency whilst the opposite is happening when antenna is twisted along its width. These results agree with our previous investigation of the impact of twisting on microstrip patch antenna operating at 2.45 GHz and fed by a microstrip line [29]. However, as the dimensions of 5.68 GHz antenna are smaller the impact of the twisting results in a smaller shift of the resonant frequency compared to the 2.45 GHz antenna.

The shaded region depicts the fractional bandwidth of 3.5% of the flat antenna and it can be seen that the deformed antenna resonant frequency stays within the bandwidth of the flat antenna. In all cases the S_{11} values at the resonant frequency tend to increase but more so for the case of twisting along the length of the antenna.

Twisting deformation along the length of antenna decreases the overall bandwidth of the antenna and has a larger impact than twisting deformation along the width of antenna as shown in Fig.14. In all cases considered the deformed antenna predominantly operates within the band defined by the flat antenna which is depicted by the shaded region in Fig.13. Twisting deformation of the antenna tends to average the effective dielectric constant and the impact of the fringing fields so that the overall impact of the deformation on the bandwidth and the resonant frequency of antenna is smaller compared to other deformations investigated in this paper which is also confirmed in [17,27].

The impact of the twisting deformation on the far field radiation pattern is shown in Fig.15. Fig.15(a) compares the E-plane radiation pattern of the flat patch antenna (solid line) with the deformed antenna for maximum twisting parameter considered in this paper i.e., 0.0125 twist/m. Fig.15(b) shows the same information but for the H-plane radiation pattern. Comparing Fig.15(a) and Fig.15(b) it can be seen that twisting antenna along its length has much bigger impact on the antenna radiation pattern, both in the terms of the main beam and also in the increased back radiation compared to the case when twisting is induced along the width of antenna.

D. Comparison with the Cylindrical Deformations

An important question to consider is how the results from the previous section compare with those of representative one-dimensional (1D) cylindrical deformations along the cylinder plane and whether it is enough to just consider simpler 1D deformations in order to assess antenna stability under deformations. To answer this question this section compares the impact of 2D spherical deformations on antenna performance against the cylindrical deformation along both E and H- plane. GC cage of the cylindrical deformation is controlled by the cylinder radius that is varied from 20 to 50 mm. Four cases are considered, namely concave and convex cylindrical bending, each along both the length and the width of antenna.

Fig.16 compares the impact of the spherical concave deformations on antenna resonant frequency and S_{11} parameter against the concave cylindrical deformations along the length and width of antenna. Our results for concave cylindrical bending agree with majority of published literature that state that bending along the length of antenna results in the increase

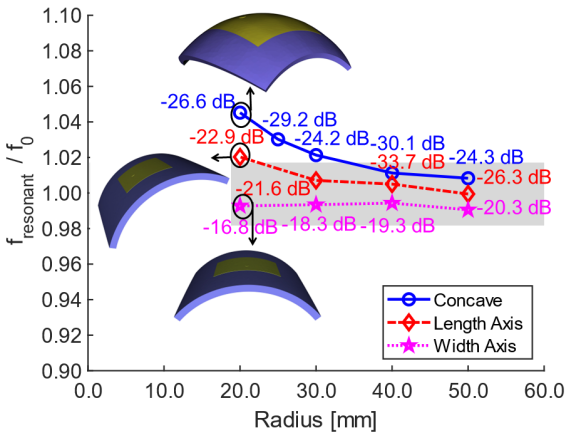

Fig. 16. Change in the resonant frequency of deformed antenna compared to the flat antenna for the concave spherical and length and width axis cylindrical bending. Values (dB) indicate the value of S_{11} parameter at the resonant frequency and the shaded region indicates the 3.5% fractional bandwidth of the flat antenna.

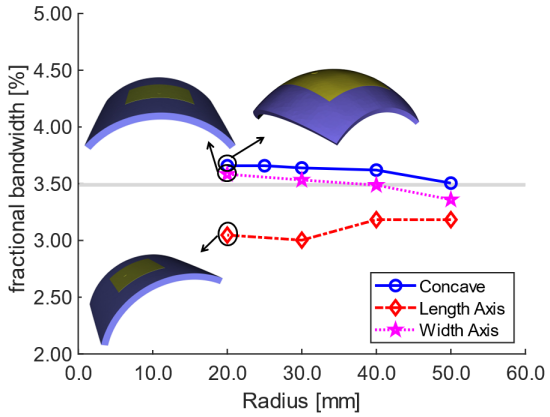

Fig. 17. The fractional bandwidth for a concave spherically deformed antenna and antenna with length and width axis.

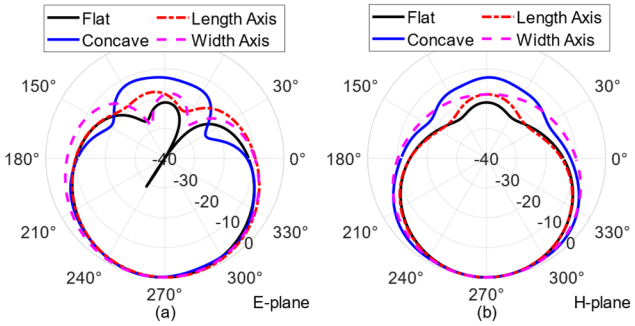

Fig.18. Comparison of the far field radiation pattern at 5.6 GHz in a) E-plane and b) H-plane of a flat patch antenna (solid line) with antenna deformed using concave deformation with radius 20mm, and respective length and width axis deformation of antenna.

of resonant frequency due to the reduced effective length of the antenna [20,21,24]. Concave bending along the width of antenna does not have much impact on the resonant frequency and has stronger impact on the bandwidth of antenna and is in agreement with [21,24].

Fig.16 shows that the impact of concave spherical deformation is more significant than representative cylindrical deformations. Whilst there seems to be a correlation between the results in the frequency shift between the cylindrical

deformation along the antenna length and spherical deformation, 1D deformations underestimate the amount of frequency shift. Furthermore, the values of the S_{11} parameter at the resonant frequency in the case of cylindrical bending tend to increase for all cases but more significantly in the case of cylindrical bending along the width of antenna, mostly due to the introduced curvature in the excitation plane. This will have most consequence for the bandwidth of antenna as explored in Fig.17 that compares the impact of concave spherical and cylindrical deformations on the antenna fractional bandwidth. The cylindrical bending along the length of antenna acts to decrease the antenna fractional bandwidth [21,24] which can be explained by the fact that the fringing fields at radiating ends of antenna are in different planes tending to decrease the bandwidth of antenna. The cylindrical bending along the width of antenna acts to increase the antenna bandwidth [21,24] as the fringing fields at radiating ends are in the same plane. Results for cylindrical bending along the width of antenna are more strongly correlated with the results of spherical bending but again, underestimate the change in bandwidth.

Comparisons of the impact of the concave spherical and cylindrical bending on the far field radiation pattern are shown in Fig.18 for the deformation radius r = 20 mm. Fig.18(a) compares the far field radiation patterns in the E-plane of the flat antenna with cylindrically deformed antenna along the length and the width axis and spherically deformed antenna. Fig.18(b) gives the same information but for the far field radiation pattern in the H-plane. It can be seen that in both cases the spherical and cylindrical deformations have similar impact on the main lobe but that spherical deformation has a much stronger impact on the back lobes.

Fig.19 compares the impact of the convex spherical deformation and the simpler cylindrical deformations on the antenna resonant frequency and the value of S_{11} at the resonant frequency. According to Fig. 18 convex cylindrical bending along antenna length acts to reduce the resonant frequency of antenna which is due to the larger effective length of antenna. Convex cylindrical bending along the width of antenna again does not have much impact on the resonant frequency. In both cases 1D convex cylindrical bending underestimate the change in the resonant frequency of antenna due to convex spherical bending. Furthermore, the S_{11} value at the resonant frequency in the case of spherical bending remains largely unaffected whilst in the case of cylindrical bending the S_{11} values increase and more so in the case of cylindrical bending along the antenna width [22] which we believe is caused by the curvature in the excitation plane. This can have potential consequences on the antenna bandwidth and this is explored in Fig.20 where impact of convex spherical and cylindrical deformations on antenna fractional bandwidth is presented.

Fig.20 demonstrates that both spherical and cylindrical deformation in the H-plane predict a reduction of antenna fractional bandwidth whilst the cylindrical bending in E-plane results in gradual increase in antenna bandwidth. Overall, cylindrical bending tends to overestimate the impact on the antenna bandwidth compared to the spherical case and this is more pronounced as the deformations are increased.

The impact of convex spherical and cylindrical bending on the

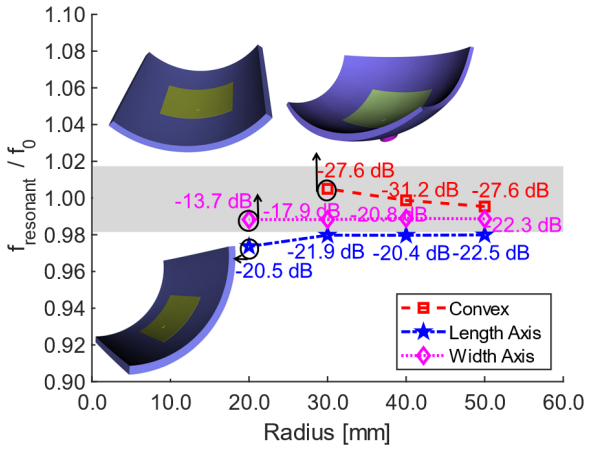

Fig. 19. Change in the resonant frequency of deformed antenna compared to the flat antenna for the convex spherical and length and width axis cylindrical bending. Values (dB) indicate the value of S_{11} parameter at the resonant frequency and the shaded region indicates the 3.5% fractional bandwidth of the flat antenna.

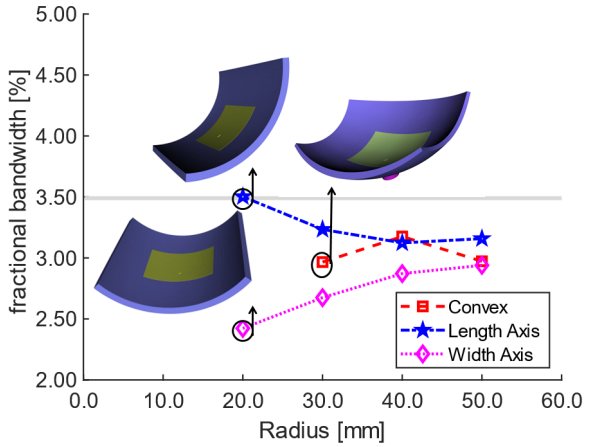

Fig. 20. The fractional bandwidth for a convex spherically deformed antenna and antenna with length and width axis cylindrical bending.

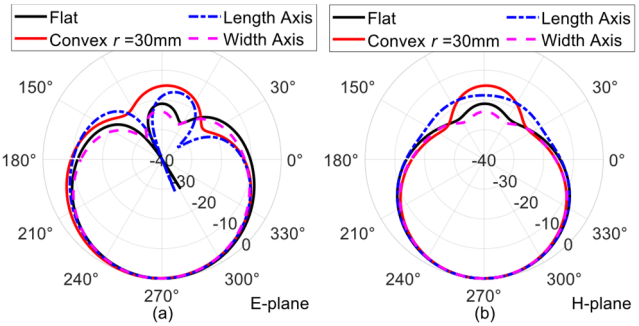

Fig. 21. Comparison of the far field radiation pattern at 5.6 GHz in a) E-plane and b) H-plane of a flat patch antenna with antenna deformed using a convex deformation with radius 30mm, and respective length and width axis deformation of antenna.

antenna far field radiation pattern is shown in Fig. 21a,b) for the case of deformation r = 30 mm and compared against the result of the flat antenna. It can be seen that the major differences are in the back lobes and that all deformations impact similarly the main radiation beam.

Overall, comparing Figs.(16-21) it can be concluded that when concave deformations are considered the spherical deformation is better correlated with the cylindrical bending

along antenna length when the impact on the resonant frequency is considered but better correlated to the cylindrical bending along the width of antenna when fractional bandwidth is considered. For the case of convex deformations, the spherical deformation is better correlated to the cylindrical bending along the width of antenna when the impact on both the resonant frequency and the bandwidth is considered. However, in each case the simpler cylindrical deformations either underestimate or overestimate the changes in antenna performance parameters by up to 4%. This is a significant observation fundamental to design. And finally, spherical convex and concave antenna deformations predict similar changes to the main beam pattern as simpler cylindrical deformations with the main changes being in the back lobes.

IV. Conclusion

This paper investigates the impact of complex deformations imposed on practical flexible antennas designed on the PDMS substrate and operating in the wireless 5.5-6 GHz region. A wide range of 2D deformations of varying strengths have been considered namely, spherical deformations, both convex and concave in nature, saddle type deformations and twisting deformations. The parameters of deformations are defined in terms of warped cages of the GC method.

Our results show that spherical bending of antenna shifts the resonant frequency of antenna to higher frequencies and that the concave spherical bending has particularly strong impact on the resonant frequency. Concave spherical deformation can act to move the bandwidth of deformed antenna outside the operating bandwidth of the flat antenna.

Saddle and twisting deformation tend to reduce the antenna resonant frequency and are more detrimental to antenna operation when deformations are applied along the length of antenna. In particular, saddle deformations where convex bending is induced along the length of antenna can reduce the resonant frequency of the antenna and move it outside the operating band designed for the flat antenna.

Our analysis and comparison of the impact of spherical bending with simpler cylindrical bending along the width and length of antenna has found that, although some correlation between results can be made when resonant frequency or bandwidth is considered, it is found that simpler cylindrical bending can underestimate or overestimate the prediction of antenna performance by up to 4%. This is deemed to be sufficiently high, and antenna can be out of the operating band designed for the flat antenna.

The presented analysis of deformed antennas shows that the GC method coupled with electromagnetic simulator is a promising design toolkit that can be confidently used to assess the impact of deformations on antenna performance and give a more accurate prediction of antenna stability under deformations.

Acknowledgment

This work was supported in part by a scholarship from Republic of Turkey Ministry of National Education and Royal Society Grant International exchanges Grant IES\R1\201311.

References

[1] A. Kumar *et al.*, "A Highly Deformable Conducting Traces for Printed Antennas and Interconnects: Silver/Fluoropolymer Composite Amalgamated by Triethanolamine", *Flexible and Printed Electronics*, vol. 2, no. 4, 2017, doi: 10.1088/2058-8585/aa8d38.

[2] R. B. V. B. Simorangkir, Y. Yang, R. M. Hashmi, T. Bjorninen, K. P. Esselle, and L. Ukkonen, "Polydimethylsiloxane-Embedded Conductive Fabric: Characterization and Application for Realization of Robust Passive and Active Flexible Wearable Antennas," *IEEE Access*, vol. 6, pp. 48102-48112, 2018, doi: 10.1109/access.2018.2867696.

[3] G. J. Hayes, J. So, A. Qusba, M. D. Dickey, and G. Lazzi, "Flexible Liquid Metal Alloy (EGaIn) Microstrip Patch Antenna", *IEEE Transactions on Antennas and Propagation*, vol. 60, no. 5, pp. 2151-2156, 2012, doi: 10.1109/TAP.2012.2189698.

[4] R. A. Liyakath, A. Takshi, and G. Mumcu, "Multilayer Stretchable Conductors on Polymer Substrates for Conformal and Reconfigurable Antennas", *IEEE Antennas and Wireless Propagation Letters*, vol. 12, pp. 603-606, 2013, doi: 10.1109/lawp.2013.2260123.

[5] I. Cherukhin, S. P. Gao, and Y. X. Guo, "Fully Flexible Polymer-based Microwave Devices: Materials, Fabrication Technique, and Application to Transmission Lines", *IEEE Transactions on Antennas and Propagation*, pp. 1-1, 2021, doi: 10.1109/TAP.2021.3083855.

[6] T. Rai, P. Dantes, B. Bahreyni, and W. S. Kim, "A Stretchable RF Antenna With Silver Nanowires", *IEEE Electron Device Letters*, vol. 34, no. 4, pp. 544-546, 2013, doi: 10.1109/led.2013.2245626.

[7] C. Lin, C. Chang, Y. T. Cheng, and C. F. Jou, "Development of a Flexible SU-8/PDMS-Based Antenna", *IEEE Antennas and Wireless Propagation Letters*, vol. 10, pp. 1108-1111, 2011, doi: 10.1109/LAWP.2011.2170398.

[8] N. J. Farcich, J. Salonen, and P. M. Asbeck, "Single-Length Method Used to Determine the Dielectric Constant of Polydimethylsiloxane", *IEEE Transactions on Microwave Theory and Techniques*, vol. 56, no. 12, pp. 2963-2971, 2008, doi: 10.1109/tmtt.2008.2007182.

[9] Y. Bonnassieux *et al.*, "The 2021 Flexible and Printed Electronics Roadmap", *Flexible and Printed Electronics*, vol. 6, no. 2, 2021, doi: 10.1088/2058-8585/abf986.

[10] Y. Wu, S. S. Mechael, and T. B. Carmichael, "Wearable E-Textiles Using a Textile-Centric Design Approach", *Acc Chem Res*, vol. 54, no. 21, pp. 4051-4064, Nov 2 2021, doi: 10.1021/acs.accounts.1c00433.

[11] A. Kiourti, C. Lee, and J. L. Volakis, "Fabrication of Textile Antennas and Circuits With 0.1 mm Precision", *IEEE Antennas and Wireless Propagation Letters*, vol. 15, pp. 151-153, 2016, doi: 10.1109/lawp.2015.2435257.

[12] A. Kiourti and J. L. Volakis, "High-Geometrical-Accuracy Embroidery Process for Textile Antennas With Fine Details", *IEEE Antennas and Wireless Propagation Letters*, vol. 14, pp. 1474-1477, 2015, doi: 10.1109/lawp.2014.2363556.

[13] K. Yan, J. Li, L. Pan, and Y. Shi, "Inkjet Printing for Flexible and Wearable Electronics", *APL Materials*, vol. 8, no. 12, p. 120705, 2020, doi: 10.1063/5.0031669.

[14] L. Song, B. Zhang, D. Zhang, and Y. Rahmat-Samii, "Embroidery Electro-Textile Patch Antenna Modeling and Optimization Strategies with Improved Accuracy and Efficiency", *IEEE Transactions on Antennas and Propagation*, pp. 1-1, 2022, doi: 10.1109/tap.2022.3145443.

[15] J. Zhu, J. J. Fox, N. Yi, and H. Cheng, "Structural Design for Stretchable Microstrip Antennas", *ACS Appl Mater Interfaces*, vol. 11, no. 9, pp. 8867-8877, Mar 6 2019, doi: 10.1021/acsami.8b22021.

[16] F. Nikbakhtnasrabadi, H. El Matbouly, M. Ntagios, and R. Dahiya, "Textile-Based Stretchable Microstrip Antenna with Intrinsic Strain Sensing", *ACS Appl Electron Mater*, vol. 3, no. 5, pp. 2233-2246, May 25 2021, doi: 10.1021/acsaelm.1c00179.

[17] J. Zhu *et al.*, "Stretchable Wideband Dipole Antennas and Rectennas for RF Energy Harvesting", *Mater Today Phys*, vol. 18, May 2021, doi: 10.1016/j.mtphys.2021.100377.

[18] J. Zhu *et al.*, "Strain-Insensitive Hierarchically Structured Stretchable Microstrip Antennas for Robust Wireless Communication", *Nanomicro Lett*, vol. 13, no. 1, p. 108, Apr 9 2021, doi: 10.1007/s40820-021-00631-5.

[19] L. Shao *et al.*, "Flexible Force Sensitive Frequency Reconfigurable Antenna Base on Stretchable Conductive Fabric", *Journal of Physics D: Applied Physics*, vol. 55, no. 19, 2022, doi: 10.1088/1361-6463/ac4f91.

[20] S. Sankaralingam and B. Gupta, "Development of Textile Antennas for Body Wearable Applications and Investigations on Their Performance under Bent Conditions", *Progress In Electromagnetics Research B*, vol. 22, pp. 53-71, 2010, doi: 10.2528/pierb10032705.

[21] D. Ferreira, P. Pires, R. Rodrigues, and R. F. S. Caldeirinha, "Wearable Textile Antennas: Examining the Effect of Bending on Their Performance", *IEEE Antennas and Propagation Magazine*, vol. 59, no. 3, pp. 54-59, 2017, doi: 10.1109/map.2017.2686093.

[22] Y. Mukai, V. T. Bharambe, J. J. Adams, and M. Suh, "Effect of Bending and Padding on the Electromagnetic Performance of a Laser-cut Fabric Patch Antenna", *Textile Research Journal*, vol. 89, no. 14, pp. 2789-2801, 2018, doi: 10.1177/0040517518801202.

[23] R. B. V. B. Simorangkir, Y. Yang, K. P. Esselle, and B. A. Zeb, "A Method to Realize Robust Flexible Electronically Tunable Antennas Using Polymer-Embedded Conductive Fabric", *IEEE Transactions on Antennas and Propagation*, vol. 66, no. 1, pp. 50-58, 2018, doi: 10.1109/tap.2017.2772036.

[24] L. Song and Y. Rahmat-Samii, "A Systematic Investigation of Rectangular Patch Antenna Bending Effects for Wearable Applications", *IEEE Transactions on Antennas and Propagation*, vol. 66, no. 5, pp. 2219-2228, 2018, doi: 10.1109/tap.2018.2809469.

[25] T. N. Kapetanakis, C. D. Nikolopoulos, K. Petridis, and I. O. Vardiambasis, "Wearable Textile Antenna with a Graphene Sheet or Conductive Fabric Patch for the 2.45 GHz Band", *Electronics*, vol. 10, no. 21, 2021, doi: 10.3390/electronics10212571.

[26] J. Zhang, J. Huang, P. Sun, F. Meng, J. Zhang, and P. Zhao, "Analysis Method of Bending Effect on Transmission Characteristics of Ultra-Low-Profile Rectangular Microstrip Antenna", *Sensors (Basel)*, vol. 22, no. 2, Jan 13 2022, doi: 10.3390/s22020602.

[27] S.-m. Sim, Y. Lee, H.-L. Kang, K.-Y. Shin, S.-H. Lee, and J.-M. Kim, "RF Performance of Ink-jet Printed Microstrip Lines on Rigid and Flexible Substrates", *Microelectronic Engineering*, vol. 168, pp. 82-88, 2017, doi: 10.1016/j.mee.2016.11.011.

[28] Vukovic, E. Altinozen, P. Sewell, I. Harrison, "*A Virtual Environment for Evaluation of Wearable Antenna Performance*", *2021 International Conference on Electromagnetics in Advanced applications*,(ICEAA), 9-13. August 2021, Honolulu, USA, USA. doi: 10.1109/ICEAA52647.2021.9539616.

[29] Vukovic, E. Altinozen, T. Dimitrijevic, P. Sewell, "*Simulation Platform for Flexible Electronics*", *15th International Conference on Advanced technologies, Systems and Services in Telecommunications (TELSIKS)*, 20-22 October 2021, Nis, Serbia, doi: 10.1109/TELSIKS52058.2021.9606324

[30] E. Altinozen, I. Harrison, A. Vukovic, and P. Sewell, "Systematic Generation of Arbitrary Antenna Geometries", *IEEE Transactions on Antennas and Propagation*, pp. 1-1, 2022, doi: 10.1109/TAP.2022.3165539.

[31] Y. Lipman, D. Levin, and D. Cohen-Or, "Green Coordinates", *ACM Trans. Graph.*, vol. 27, no. 3, pp. 1-10, 2008, doi: 10.1145/1360612.1360677.

[32] Y. Lipman and D. Levin, "Derivation and Analysis of Green Coordinates", *Computational Methods and Function Theory*, journal article vol. 10, no. 1, pp. 167-188, June 01 2010, doi: 10.1007/bf03321761.

[33] T. Ju, S. Schaefer, and J. Warren, "Mean Value Coordinates for Closed Triangular Meshes", *ACM Trans. Graph.*, vol. 24, no. 3, pp. 561–566, 2005, doi: 10.1145/1073204.1073229.

[34] M. S. Floater, G. Kós, and M. Reimers, "Mean Value Coordinates in 3D", *Computer Aided Geometric Design*, vol. 22, no. 7, pp. 623-631, 2005, doi: 10.1016/j.cagd.2005.06.004.

[35] P. Joshi, M. Meyer, T. DeRose, B. Green, and T. Sanocki, "Harmonic Coordinates for Character Articulation", *ACM Transactions on Graphics*, vol. 26, no. 99, 2007, doi: 10.1145/1276377.1276466.

[36] S. W. Cheng, T. K. Dey, and J. Shewchuk, *Delaunay Mesh Generation*. CRC Press, 2013.

[37] C. Christopoulos, *The Transmission-Line Modeling Method: TLM*. John Wiley & Sons, 1995.

[38] P. Sewell, T. M. Benson, C. Christopoulos, D. W. P. Thomas, A. Vukovic, and J. G. Wykes, "Transmission-line Modeling (TLM) Based upon Unstructured Tetrahedral Meshes", *IEEE Transactions on Microwave Theory and Techniques*, vol. 53, no. 6, pp. 1919-1928, 2005, doi: 10.1109/tmtt.2005.848078.

[39] P. D. Sewell, T. M. Benson, C. Christopoulos, D. W. P. Thomas, A. Vukovic, and J. G. Wykes, "Implicit Element Clustering for Tetrahedral Transmission-Line Modeling (TLM)", *IEEE Transactions on Microwave Theory and Techniques*, vol. 57, no. 8, pp. 2005-2014, 2009, doi: 10.1109/tmtt.2009.2025451.

[40] X. Meng, A. Vukovic, T. M. Benson, and P. Sewell, "Extended Capability Models for Carbon Fiber Composite (CFC) Panels in the Unstructured Transmission Line Modeling (UTLM) Method", *IEEE Transactions on Electromagnetic Compatibility*, vol. 58, no. 3, pp. 811-819, 2016, doi: 10.1109/temc.2016.2531791.

[41] A. Vukovic, P. Sewell, X. Meng, and T. M. Benson, "Installed Antenna Performance in Airborne Radomes of Different Profiles", No.3, Vol.33, pp.343-346, 2018.

[42] A. Vukovic, P. Sewell, and T. M. Benson, "Holistic Appraisal of Modeling Installed Antennas for Aerospace Applications", *IEEE Transactions on Antennas and Propagation*, vol. 67, no. 3, pp. 1396-1409, 2019, doi: 10.1109/tap.2018.2884769.

[43] P. Sewell, A. Vukovic, T. M. Benson, and X. Meng, "Extracting Modal Field Profiles from 3D Unstructured Transmission Line Modelling Meshes for Use as Sources and Observers", *IET Science, Measurement & Technology*, vol. 11, no. 6, pp. 780-785, 2017, doi: 10.1049/iet-smt.2016.0357.

Ekrem Altinozen received a B.Sc. degree in electrical and electronic engineering from Eskisehir Osmangazi University, Eskisehir, Turkey, in 2015, and a M.Sc. degree (with first-class honors) from The University of Nottingham, Nottingham, U.K. in 2018, where he is currently pursuing a Ph.D. degree. His current research interests are conformal, wearable and foldable antennas and interconnects for personal and industrial applications.

Ana Vukovic (M'97) was born in Nis, Serbia, in 1968. She received the Diploma of Engineering degree in electronics and telecommunications from the University of Nis, Nis, Yugoslavia, in 1992, and the Ph.D. degree from the University of Nottingham, Nottingham, U.K., in 2000. From 1992 to 2001, she was a Research Associate with the University of Nottingham. In 2001, she joined the School of Electrical and Electronic Engineering, University of Nottingham, as a Lecturer. In 2019 she became a Professor of Electromagnetics applications. Her research interests are electromagnetics with a particular emphasis on applications in optoelectronics, microwaves, and EMC.

Phillip Sewell (M'89-SM'04) was born in London, U.K., in 1965. He received the B.Sc. degree in electrical and electronic engineering (with first-class honors) and Ph.D. degree from the University of Bath, Bath, U.K., in 1988 and 1991, respectively. From 1991 to 1993, he was a Post-Doctoral Fellow with the University of Ancona, Ancona, Italy. In 1993, he became a Lecturer with the School of Electrical and Electronic Engineering, University of Nottingham, Nottingham, U.K. In 2001 and 2005, he became a Reader and Professor of electromagnetics at the University of Nottingham. His research interests involve analytical and numerical modeling of electromagnetic problems with application to opto-electronics, microwaves and aerospace applications.